Chin. J. Astron. Astrophys. Vol. 4 (2004), No. 4, 365–376
(http://www.chjaa.org or http://chjaa.bao.ac.cn)

Chinese Journal of Astronomy and Astrophysics

Calibration of Vector Magnetogram with the Nonlinear Least-squares Fitting Technique *

Jiang-Tao Su and Hong-Qi Zhang

National Astronomical Observatories, Chinese Academy of Sciences, Beijing 100012;
sjt@sun10.bao.ac.cn

Received 2003 November 16; accepted 2004 April 30

Abstract To acquire Stokes profiles from observations of a simple sunspot with the Video Vector Magnetograph at Huairou Solar Observing Station (HSOS), we scanned the FeI λ5324.19 Å line over the wavelength interval from 150 mÅ redward of the line center to 150 mÅ blueward, in steps of 10 mÅ. With the technique of analytic inversion of Stokes profiles via nonlinear least-squares, we present the calibration coefficients for the HSOS vector magnetic magnetogram. We obtained the theoretical calibration error with linear expressions derived from the Unno-Becker equation under weak-field approximation.

Key words: Sun: activity — Sun: magnetic fields — sunspots

1 INTRODUCTION

We use the data of vector magnetic fields obtained by the imaging vector magnetograph on the Solar Magnetic Field Telescope of the Huairou Solar Observing Station (HSOS) of the National Astronomical Observatories of China. The data are normally in the form of the Stokes polarization images in portions of the spectral line obtained using a birefringent filter (1/8 Å bandpass). The working line is FeI λ5324.19 Å for the photospheric magnetic field measurements. The equivalent width of the line is 0.33 Å and the Landé factor $g = 1.5$. For measurement of the longitudinal field, the filter is tuned to –0.075 Å of the line center, which is the optimum place for the coefficient of calibration with both moderate sensitivity and linearity (Wang, Ai & Deng 1996). Ai et al. (1982) pointed out that the linearity was best when calibrating the transverse field at $\pm 0.10 \sim \pm 0.11$ Å from the line center. However, for the well-known reason that cross-talk effects are weakest at the line center, the measurement of transverse field is taken at the line center.

To reconstruct the vector magnetogram, we use the linear relations between the magnetic field and the Stokes parameters I, Q, U and V established under the condition of weak-field approximation,

$$B_{\parallel} = C_{\parallel} \frac{V}{I}, \qquad B_{\perp} = C_{\perp} \left[\left(\frac{Q}{I} \right)^2 + \left(\frac{U}{I} \right)^2 \right]^{1/4}, \tag{1}$$

where $C_{\parallel}$ and $C_{\perp}$ are the calibration coefficients for the longitudinal and transverse magnetograms, respectively. The theoretical calibration for HSOS vector magnetogram was first made

* Supported by the National Natural Science Foundation of China.

by Ai et al. (1982) using the early solar atmosphere models given by Allen (1973). The results indicated that the calibration coefficients were sensitive to the atmosphere models. For routine observations, an empirical calibration is used by adopting the standard line profile observed at Kitt Peak, instead of solving the Unno-Beckers equation. The calibration coefficients $C_{\|}$ and $C_{\perp}$ are 10.00×10^3 and 9.73×10^3 G for the longitudinal and transverse magnetic fields, respectively (Wang et al. 1996). Wang, Ai & Deng (1996) used two methods to calibrate the longitudinal magnetograms, an empirical calibration, a velocity calibration and $C_{\|}$ were found to be 8.88×10^3 G with the former and 9.60×10^3 G with the latter. However, their measurements were all restricted to solar quiet regions. In this paper, our observations are made on a sunspot.

The Stokes profiles were obtained by scanning each wavelength of the FeIλ5324.19 Å line with the vector magnetograph system on HSOS. Such an effort was first made with the Mashell Space Flight center system for observations of a sunspot (Balasubramaniam & West 1991). We try to obtain the calibration coefficients for the longitudinal and transverse fields by recovering the vector magnetic field parameters and other physical parameters with the nonlinear least-squares technique of analytic inversion of the Stokes profiles.

2 OBSERVATIONS AND DATA REDUCTION

The observational data were obtained on 2003 October 23, with the HSOS vector magnetograph for a relative simple sunspot in the super active region NOAA 10484 located at N04 E12.4. The observations can be divided into two categories: spectral scan data and standard deviation data. The spectral scan data were Stokes images extending from –150 mÅ in the blue wing to +150 mÅ in the red wing of the FeI λ5324.19 Å line at steps of 10 mÅ. First the V/I image was acquired; next the Q/I image, followed by the U/I image. The time required to obtain a set of Stokes images was about 1 minute for each spectral location. The standard deviation data were Stokes images observed at $\pm$60 mÅ from the line center and 10 sets of such data were obtained. Each image was a 256-frame integration. The observations were carried out from 01:00 to 02:20 UT.

The cross-talk corrections are shown in Fig. 1, over the entire field of view. A linear fit of the data is sufficient. A scatter plot of the standard deviation in the polarization signals as a function of the polarization intensity is shown in Fig. 2 for the sunspot penumbra. The Stokes intensities Q, U, and V at each of the 31 filter positions were registered with the data set taken at 75 mÅ to the blue of the line center.

We also present three vector magnetograms in Fig. 3: the top one was obtained by superposing the azimuths observed at 120 mÅ in the blue wing (thin line) on those observed at the line center (thick line) and the figure was corrected for cross-talk effects; the middle one and the bottom one were obtained by superposing the azimuths observed at 120 mÅ (thin line) in the blue wing on those observed at 120 mÅ in the red wing (thick line) without and with cross-talk corrections, respectively. The three plots were superposed on the line of sight magnetogram observed at –75 mÅ from the line center.

Figure 3b shows that the red and blue transverse magnetograms differ obviously in both azimuth and magnitude. After the cross-talk corrections, the differences between the two magnetograms become trivial, as shown in Fig. 3c. For some pixels of the inner umbra, however, a magnitude difference still remains. This is ascribed mainly to the asymmetric character of the FeIλ5324.19 Å line in the two wings when observed in the umbra (Wallace et al.). So

we omit some data of the inner umbra in the following analysis. The azimuth differences ($\phi_{0.00\text{Å}} - \phi_{-0.12\text{Å}}$) of the first panel were mainly caused by magneto-optical effects while the differences ($\phi_{0.12\text{Å}} - \phi_{-0.12\text{Å}}$) of the third panel were mainly caused by cross-talk effects. The mean value is 14.1° for the former and 7.3° for the latter. These results may serve as an evidence that measurements of the transverse fields should be made at the far wings of the spectral line even though the cross-talk effects there are more serious.

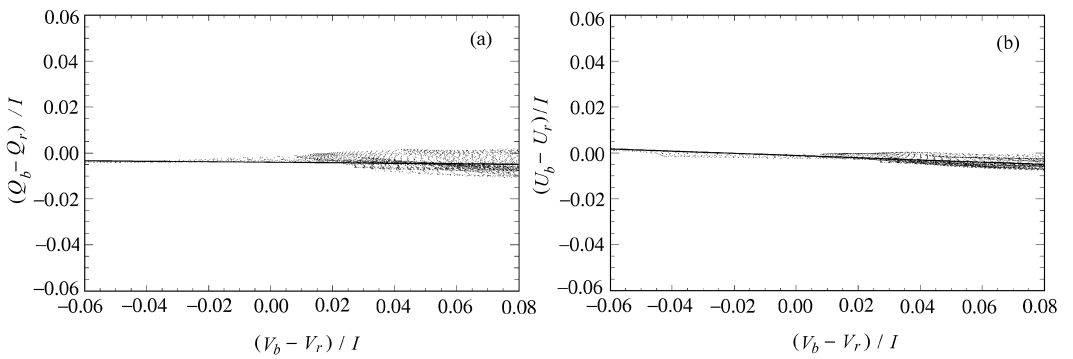

Fig. 1 Polarization cross-talk introduced by the polarimeter and sample scatter plots derived from one set of ±60 mÅ data. Scatter plot of Stokes $(Q_b - Q_r)/I$ vs. $(V_b - V_r)/I$ is shown on (a) plot and scatter plot for $(U_b - U_r)/I$ vs. $(V_b - V_r)/I$ is shown at (b) plot. The solid lines in two plots represent the linear fits to the data.

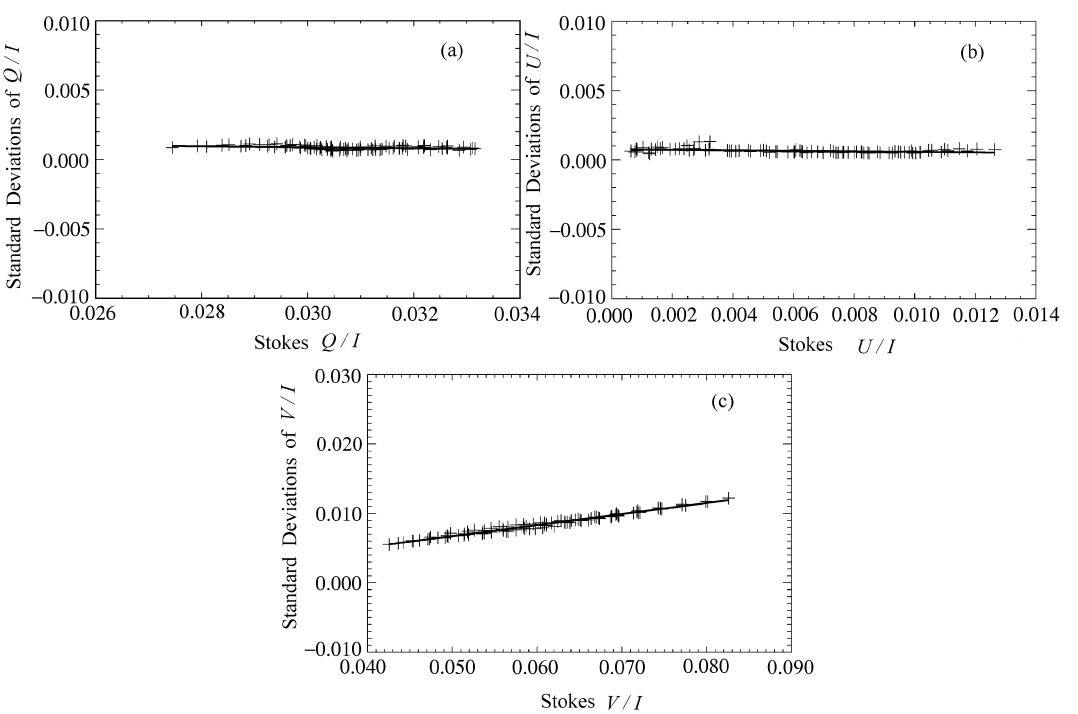

Fig. 2 Scatter plots of the standard deviation in the linear and circular polarization as a function of the polarization intensity for the penumbra. The solid lines in the figure represent the linear fits. The standard deviation is symmetric about zero for the negative polarization.

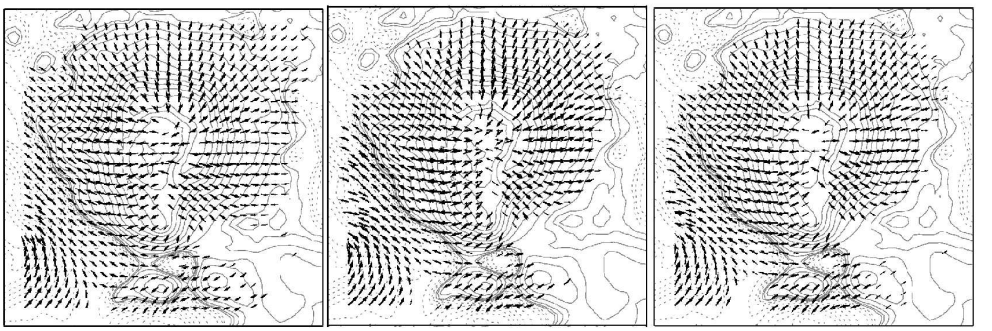

Fig. 3 Three bird-foot vector magnetograms of a simple sunspot of NOAA 10484 on 2003 October 23, the field of view is 84×84 arcsec. North is up and west is to the right. (a) The azimuths observed at 120 mÅ to the blue of the line center (thin line) superposed on the azimuths from observations at the line center (thick line) and the cross-talk corrections were applied. (b) The azimuths observed at ±120 mÅ from the line center. The thin line is for the blue wing and the thick one for the red wing. (c) Similar to the middle panel, but with the cross-talk corrections applied.

3 ANALYTICAL SOLUTION OF STOKES PROFILES

The analytical solutions of the Stokes profiles as derived by Landofi & Landi Degl'Innocenti (1982) are

$$\begin{aligned} I &= B_0 + \frac{uB_1}{\Delta}\{(1+\eta_I)[(1+\eta_I)^2 + \rho_Q^2 + \rho_U^2 + \rho_V^2]\}, \\ Q &= -\frac{uB_1}{\Delta}[(1+\eta_I)^2\eta_Q + (1+\eta_I)(\eta_V\rho_U - \eta_U\rho_V) + \rho_Q R], \\ U &= -\frac{uB_1}{\Delta}[(1+\eta_I)^2\eta_U + (1+\eta_I)(\eta_Q\rho_V - \eta_V\rho_Q) + \rho_U R], \\ V &= -\frac{uB_1}{\Delta}[(1+\eta_I)^2\eta_V + \rho_V R], \end{aligned} \tag{2}$$

where

$$\begin{aligned} I &= (1+\eta_I)^2[(1+\eta_I)^2 - \eta_Q^2 - \eta_U^2 - \eta_V^2 + \rho_Q^2 + \rho_U^2 + \rho_V^2] - R^2, \\ R &= \eta_Q\rho_Q + \eta_U\rho_U + \eta_V\rho_V. \end{aligned} \tag{3}$$

Here $\mu = \cos\theta$, θ is the angle between the line of sight and the normal to the solar surface. The absorption profiles $\eta_{I,Q,U,V}$ and the dispersion profiles $\rho_{Q,U,V}$ are given by

$$\begin{aligned} \eta_I &= 0.5[\eta_p \sin^2\psi + 0.5(\eta_b + \eta_r)(1 + \cos^2\psi)], \\ \eta_Q &= 0.5[\eta_p - 0.5(\eta_b + \eta_r)]\sin^2\psi\cos 2\phi, \\ \eta_U &= 0.5[\eta_p - 0.5(\eta_b + \eta_r)]\sin^2\psi\sin 2\phi, \\ \eta_V &= 0.5(\eta_r - \eta_b)\cos\phi, \\ \rho_Q &= 0.5[\rho_p - 0.5(\rho_b + \rho_r)]\sin^2\psi\cos 2\phi, \\ \rho_U &= 0.5[\rho_p - 0.5(\rho_b + \rho_r)]\sin^2\psi\sin 2\phi, \\ \rho_V &= 0.5(\rho_r - \rho_b)\cos\phi, \end{aligned} \tag{4}$$

where ψ is the inclination and ϕ is the azimuth of the magnetic field vector. For a normal Zeeman triplet, the absorption profiles and the anomalous dispersion profiles are

$$\begin{aligned} \eta_p &= \eta_0 H(a,v), \quad & \rho_p &= 2\eta_0 F(a,v); \\ \eta_{b,r} &= \eta_0 H(a,v \pm v_H), \quad & \rho_{b,r} &= 2\eta_0 F(a,v \pm v_H). \end{aligned} \tag{5}$$

Here a is the damping parameter of the spectral line, η_0 is the ratio of the line center to the continuum opacity, and

$$v = \frac{\lambda - \lambda_0}{\Delta\lambda_D} \tag{6}$$

is the separation of wavelength λ from the the line-center wavelength λ_0 in units of the Doppler width λ_D. The Zeeman splitting v_H in field of H in units of the Doppler width, is

$$v_H = \frac{(4.67^{-13}\lambda^2 g_J H)}{\Delta\lambda_D}\ , \tag{7}$$

where g_J is the Landé factor. The Faraday $F(a,v)$ and Faraday-Voigt $H(a,v)$ functions are explicitly given by

$$\begin{aligned} H(a,v) &= \frac{a}{\pi}\int_{-\infty}^{\infty} \frac{e^{-y^2}}{(v-y)^2 + a^2} dy, \\ F(a,v) &= \frac{1}{2\pi}\int_{-\infty}^{\infty} \frac{(v-y)e^{-y^2}}{(v-y)^2 + a^2} dy. \end{aligned} \tag{8}$$

The analytical solutions should be convolved with the the filter transmission function. If $S(\lambda)$ stands for the line profile of any one of the Stokes parameters, and $T(\lambda,\ \lambda')$ the transmission profile of the filter, where λ' being the bandpass location relative to the line center, then the intensity of the transmitted Stokes parameter is

$$\overline{S}(\lambda') = \int_{-2\Delta\lambda}^{2\Delta\lambda} S(\lambda)T(\lambda,\lambda')d\lambda \Big/ \int_{-2\Delta\lambda}^{2\Delta\lambda} T(\lambda,\lambda')d\lambda, \tag{9}$$

where $\Delta\lambda$ is large enough so that the integration adequately covers the whole Stokes line profile.

4 NONLINEAR LEAST-SQUARES FITTING

In this paper, the least-squares fitting technique (the chi-squared fit) is used for the broad-band resolution Stokes Q, U, and V profiles. The Stokes I profile is not used in the fitting process. The eight parameters used to optimally fit the analytical profiles to the observed profiles are the line center (λ_0), the Doppler width ($\Delta\lambda_D$), the damping constant (a), the slope of the source function ($\mathrm{uB_1}$), the opacity ratio (η_0), the total magnetic field strength (H), the inclination and azimuth of the magnetic field vector (ψ) and (ϕ). All the above parameters are treated as independent parameters. We also assume that the spectral lines are symmetric. For our purposes, chi-square is defined as

$$\begin{aligned} \chi^2 = \sum_i & \frac{1}{\sigma_{Q_i}^2}[Q_i(\mathrm{obs}) - \mathrm{Q_i(a_j;fit)}]^2 \\ & + \frac{1}{\sigma_{U_i}^2}[U_i(\mathrm{obs}) - \mathrm{U_i(a_j;fit)}]^2 \\ & + \frac{1}{\sigma_{V_i}^2}[V_i(\mathrm{obs}) - \mathrm{V_i(a_j;fit)}]^2. \end{aligned} \tag{10}$$

Summation over all the wavelength points is indicated by the index i. Here a_j refers to all the parameters that enter the Stokes Q, U, and V profiles. The weighting functions σ refer to the standard deviation (see Fig. 2). For a detailed presentation of the fitting method please refer to Balasubramaniam & West (1991).

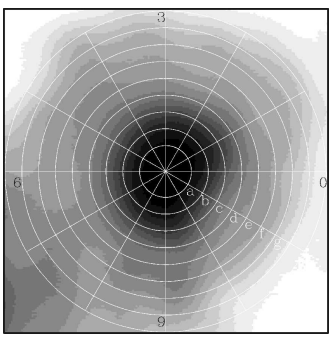

Fig. 4 Map of the sunspot's photometric intensity showing radials and circles for the selection of the pixels used in the analysis. Here a, b, c, d, e, f and g refer to the first seven intersections of radial 11 with the circles.

We adopted the method of Hagyard et al. (2000) to select the pixels for the analysis. That is, first choose 12 radial lines from the center of the umbra at 30° intervals, next choose nine circles concentric with respect to the center of the umbra, but excluding a portion of inner umbra. The intersections of the radial lines and circles define the 108 pixels selected (Fig. 4). The minimum transverse field strength obtained by the fitting is 220 G; while the minimum longitudinal component is 49 G in all the data. In Fig. 5, we present the observed Stokes profiles of Q/I, U/I, and V/I, and the model fits as functions of $\Delta\lambda$ for seven pixels of radial 11.

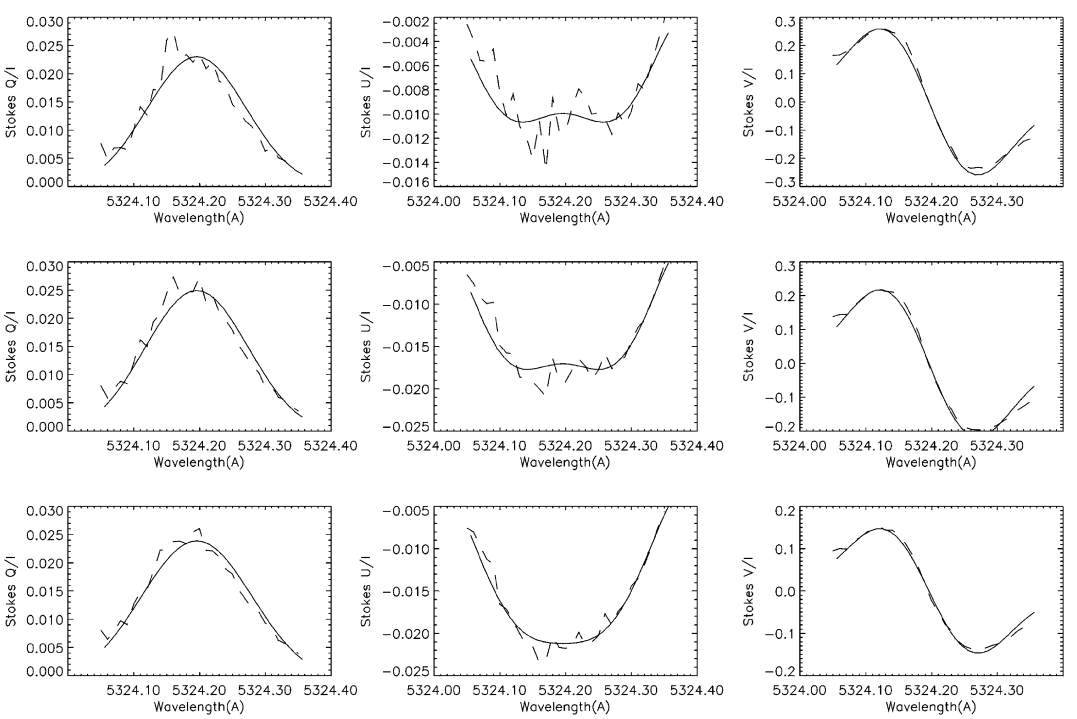

Fig. 5 Observed Stokes profiles of Q/I, U/I, and V/I for the seven pixels marked a, b, c, d, e, f and g in Fig. 4. The profiles acquired with the HOSO vector magnetograph (dashed line) in the sunspot umbra are compared with the fitted profiles resulting from the nonlinear least-square inversion (solid lines).

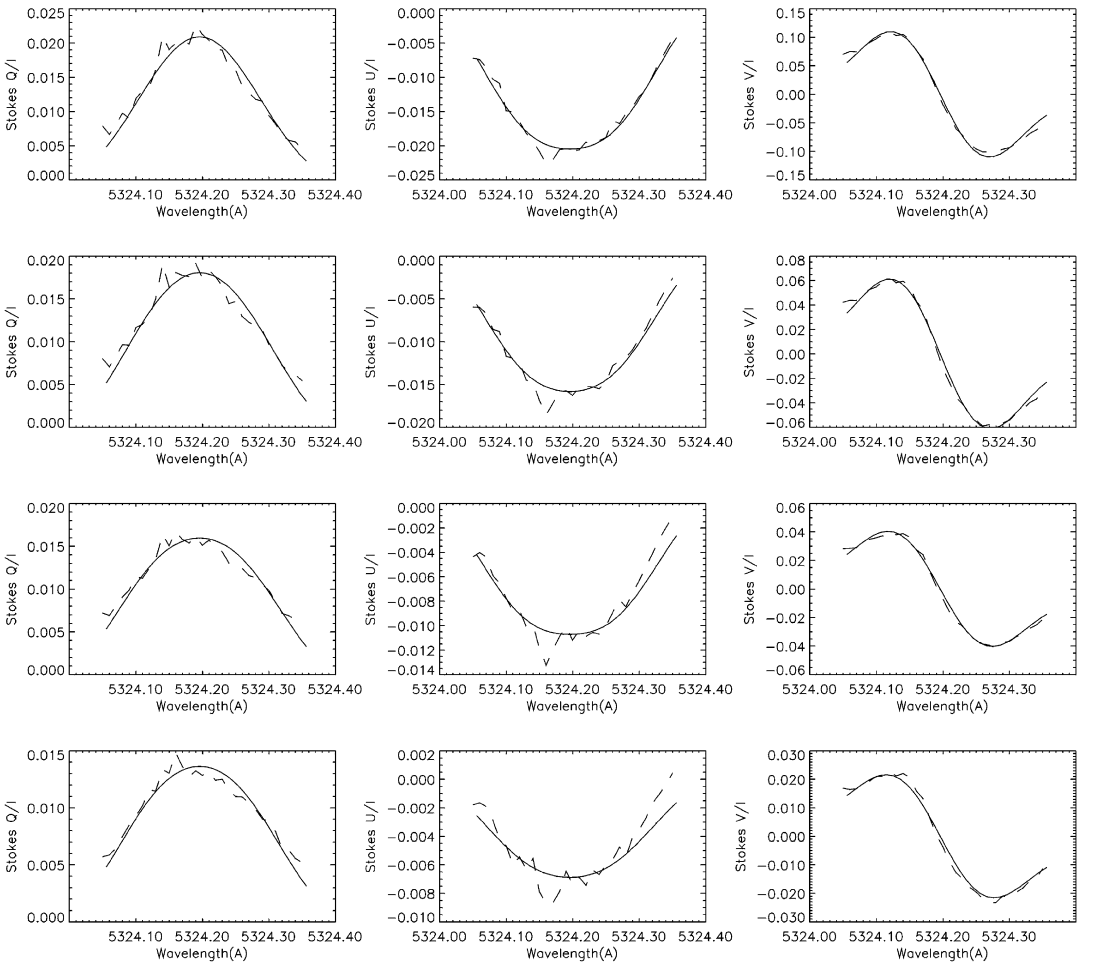

Fig. 5 Continued.

We use the best-fit model values Q/I, U/I and V/I of each analysed pixel instead of the observed values to calculate the quantity η and Stokes V/I. In Fig. 6, we plot η against the transverse field strengths $B_\perp$, η being the linear polarized intensity $100 \times [(Q/I)^2 + (U/I)^2]^{1/4}$. In Fig. 7 we plot the Stokes V/I, at –0.12 Å and –0.075 Å from the line center against the longitudinal field strengths $B_\parallel$. The calibration coefficients $C_\parallel$ and $C_\perp$ for the different offsets of filter bandpass are listed in the Table 1. Note that $C_\perp$ has been multiplied by a factor of 100, coming from the parameter η ($100 \times [(Q/I)^2 + (U/I)^2]^{1/4}$).

Table 1 Calibration Coefficients Based on Least-square Fitting

component	Bandpass (Å)	Coefficient (G)
$B_\perp$	–0.12	10550 ± 92
$B_\perp$	0.00	6790 ± 52
$B_\parallel$	–0.12	10076.5 ± 134.3
$B_\parallel$	–0.075	8381.0 ± 159.1

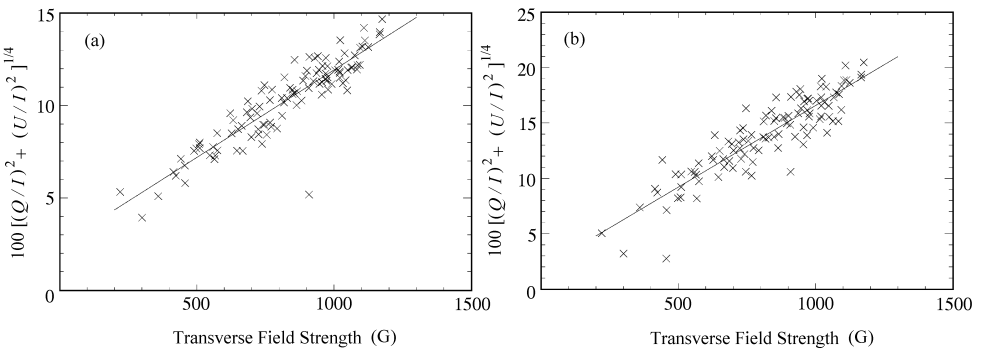

Fig. 6 Correlation plots between the linear polarized intensity quantity η and the transverse field. (a) η observed at –0.12 Å from the line center. (b) η observed at the line center. The solid lines are the linear fits.

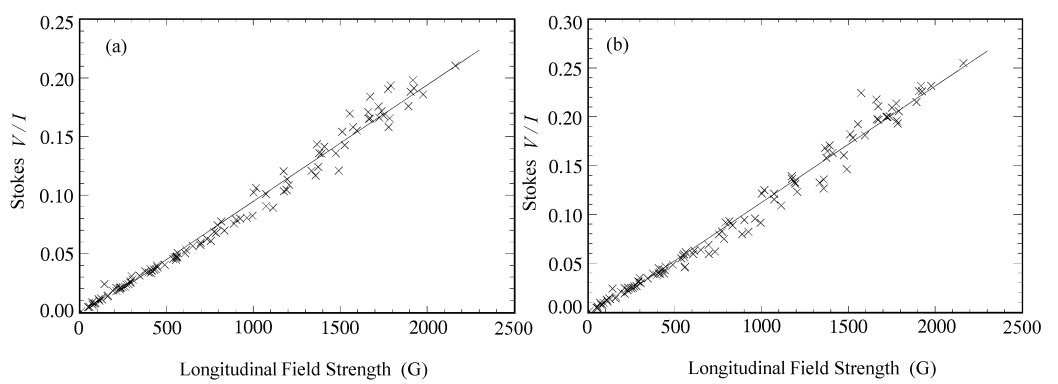

Fig. 7 Same as Fig. 6, but for the correlation between Stokes V/I and longitudinal field strengths.

5 DISCUSSION

We examine the fitting accuracies of the field strength, inclination, and azimuth of the magnetic field vector. Let $\boldsymbol{a}_{\rm true}$ and $\boldsymbol{a}_0$ be the true and fitted parameters and let $\boldsymbol{D}_0$ be the measured data set used in the fitting. Because of random measuring errors there are infinitely many realizations of the measured data set $\boldsymbol{D}_i$. Each one corresponds to a slightly different set of fitted parameters $\boldsymbol{a}_i$. We assume that the probability distribution of $\boldsymbol{a}_i - \boldsymbol{a}_0$ has the same shape as that of $\boldsymbol{a}_{\rm true} - \boldsymbol{a}_0$. We use the Monte Carlo method to generate the "hypothetical data set" of Stokes profiles subjected to varying levels of random noise (see Numerical Recipes in Fortran Second Edition, The Chapter 15, p.684). Thus a series of fitted parameters $\boldsymbol{a}_i$ was

obtained with which we can estimate the errors. Take pixel 3 in radial 11 shown in Fig. 5 as an example, the error in the magnetic field strength is $\approx 3.2\%$, the error in the inclination is $\approx 2.2\%$, the error in the azimuth is $\approx 0.3\%$. The errors of the other parameters are as follows: line center wavelength $\approx 1.6 \times 10^{-6}\%$, Doppler width $\approx 3.8\%$, opacity ratio $\approx 32\%$, damping constant $\approx 12\%$, and slope of source function $\approx 5\%$.

From the total magnetic field strength (H), its inclination (ψ) and azimuth (ϕ), we calculate the longitudinal and transverse magnetic field strength (B_L) and (B_T)

$$B_L = H\cos\psi \ ; \ B_T = H\sin\psi. \tag{11}$$

Since only the Q, U, and V profiles are used in the fitting, the filling factor is not taken into account. Therefore the field strengths are not absolute strengths, but only fluxes. The effects of scattered light are partially taken into account by using the measured standard deviations of the umbra and penumbra, separately in the chi-squared fitting. Through extensive numerical simulations, Lites & Skumnaich (1985) found that the magnetic field strength and direction are much less sensitive to the measurement error than that of the parameters that represent the local thermodynamic state of the atmosphere.

Other physical parameters resulting from the nonlinear least-square inversion fitting such as the Doppler width, opacity ratio, damping constant, and slope of the source function could, in some instances, be physically unrealistic. For example, the damping constant falls to very low value (~ 0) or rises to very high values (~ 4), and the opacity ratio varies from as low as unity to as high as 600. Physically we know that the Doppler width is a function of both the temperature and the micro-turbulent velocity; the opacity ratio is related in a complicated way to the temperature and the number density of atoms and is inversely proportional to the Doppler width (see Landi Degl'Innocenti (1976) for explicit expressions of these quantites). Breaking down these parameters into smaller units may help us to resolve their interdependence (Balasubramaniam & West 1991).

The spectral line FeI λ5324.19 Å observed in the umbra is asymmetric in the two wings as shown in Fig. 8, whereas this line is symmetric when observed in the photosphere (Wallace et al.). It is believed that the asymmetry is due to velocity gradient in the spot (see Skumnanich, Rees & Lites 1985). A rough ratio of polarized signal Q or U (150 mÅ red to 150 mÅ blue) of only 1.5 is estimated in the FeIλ5324.19 Å line (Fig. 7). As shown in the third panel of Fig. 4, the asymmetry of the two transverse field magnitudes is not so significant except in the inner umbra region. However, if velocity gradients do in fact present a problem in this method, they should be dealt with in some way by the inversion scheme to improve the fitting accuracy.

The major drawbacks of the fitting are that only the strong fields of sunspots can be derived, and that the process of obtaining the data is time-consuming compared to the usual method of observing at only a few wavelengths with the vector magnetograph. For our data, the minimum $B_\perp$ obtained is 220 G and the minimum $B_\parallel$ is 49 G. The calibration results may interpret weaker field improperly, especially in areas of the photosphere. Moreover, we do not know exactly whether these results can interpret the magnetic field of the inner umbra because the fitting process involved subtraction of the central part of the umbra. In the following we will give a theoretical discussion on the linear calibrating accuracy. Under the weak-field condition, we have two approximate formulae from the Stokes transfer equations :

$$\begin{aligned} B_\parallel &\propto V(\frac{\partial I}{\partial \nu})^{-1}, \\ B_\perp &\propto (Q^2+U^2)^{1/4}(\frac{\partial I}{\partial \nu})^{-1/2}, \end{aligned} \tag{12}$$

which provide a basis for calibrating the magnetic fields. However, in so doing, there exist two sources of error: one is the nonlinear term $\partial I/\partial\nu$ and the other is the magnetic saturation effect. When B is weak, $\partial I/\partial\nu$ is the main contributor of error; when B is very strong, the saturation effect is the main contributor. We are not able to separate these two errors, so we take them as one nonlinear error (NLE). As for longitudinal field measurements, there is another kind of error introduced by the line of sight velocity of the sunspot if the observations are taken at a fixed bandpass such as –0.075 Å from the line center. Given a typical velocity of 1km s^{-1} (Ai et al. 1982), we can obtain the wavelength shifts $\Delta\lambda = \pm 0.0175$ Å (relative to the place of –0.075 Å from the line center). The actual wavelength shifts (relative to the line center) due to Doppler movements are approximately in the range of $-0.095\,\text{Å} < \Delta\lambda < -0.055\,\text{Å}$. The formula for the error in redshift is

$$\Delta B = (-V/I_{-0.075} + V/I_{-0.095}) \times (C_{\|-0.075} - C_{\|-0.095}), \tag{13}$$

the sign is plus if V/I is positive. Similarly, for blueshift, the formula is

$$\Delta B = (-V/I_{-0.075} + V/I_{-0.055}) \times (C_{\|-0.055} - C_{\|-0.075}), \tag{14}$$

and the sign is minus if V/I is positive.

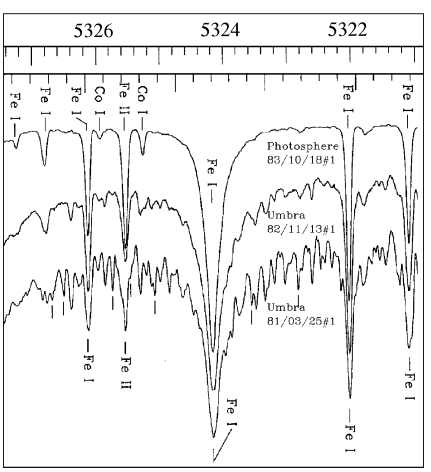

Fig. 8 A portion of the spectra line FeI5324.19 Å from Kitt Peak observations.

In Fig. 9, we present theoretical calibrating curves of the longitudinal field and the linear deviation curves for the different atmosphere models. The dashed line is for the Allen umbra model (Allen 1973), dotted line for the Ding and Fang (DF) penumbra model (Ding & Fang 1989) and solid line for the VAL-C quiet photosphere model (Vernazza et al. 1981). The solid straight lines in the plot are the linear fits of the curves. The linear deviation error and the error made by the line of sight velocity of the sunspot are listed in Table 2 and the bandpass is at –0.075 Å from the line center. The maximum calibration error is below ~ 200 G when $B_\| = 3000$ G. Similarly, in Fig. 10, we present the theoretical calibrating curves of the transverse field and the linear deviation curves for different atmosphere models. The linear deviation errors are listed in Table 3 and the bandpass is at the line center.

Table 2 Theoretical Calibration Errors for the Longitudinal Field

Model	NLE (G)	Redshift (G)	Blueshift (G)	Superposition (G)
Allen	180.5	24.8	–179	205 or 1.3
DF	130.5	61	–221	192 or –90.5
VAL-C	117	71.6	–238	189 or –121

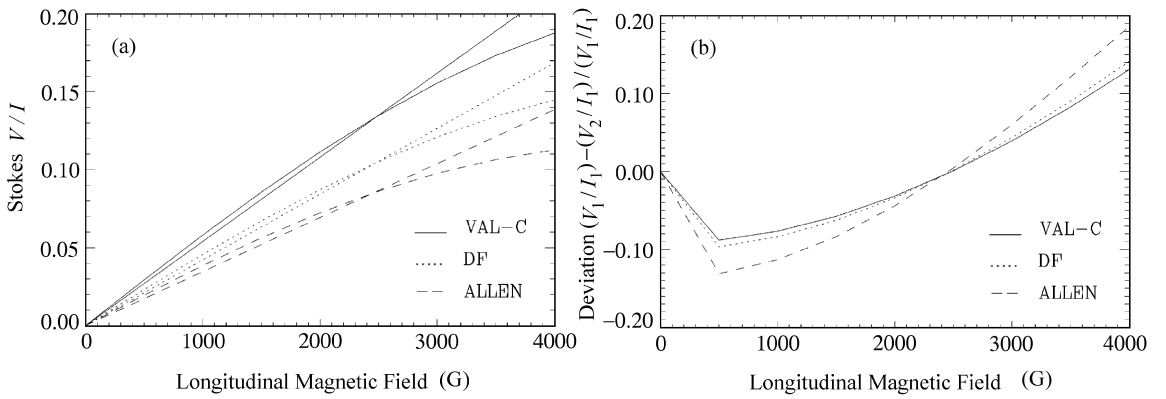

Fig. 9 (a) Theoretical calibrating curves for the longitudinal magnetic field. Bandpass at –0.075 Å from the line center for the Allen umbra, DF penumbra, and VAL-C quiet photosphere models. (b) Linear deviating curves in units of linear fitting values.

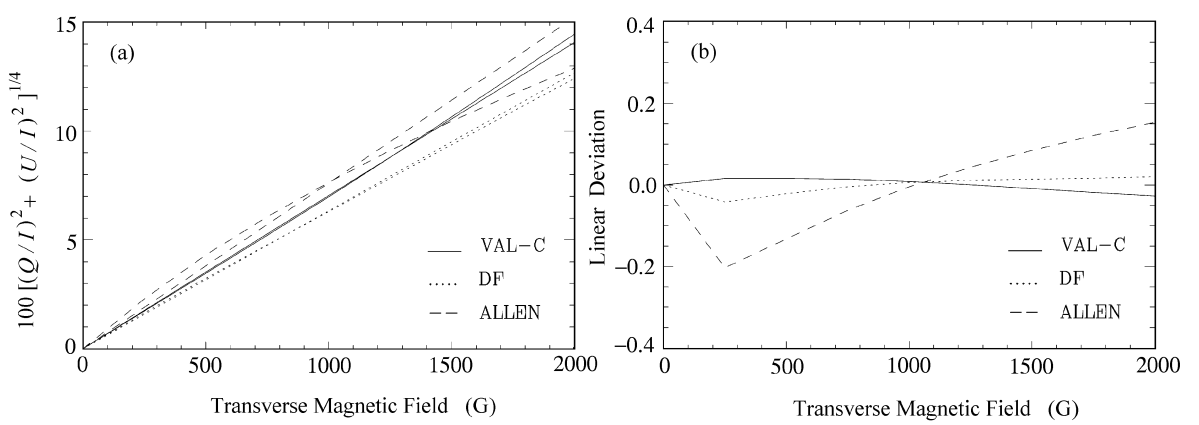

Fig. 10 Same as Fig. 9 but for the transverse field and with the bandpass at the line center.

Comparing with the empirical calibration coefficients given by Wang et al. (1996), we find our results $C_{\|} = 8381$ and $C_{\perp} = 6790$ are smaller by 10000 and 9730, respectively. In comparison with the longitudinal field calibrating coefficients given by Wang, Ai & Deng (1996), our value of $C_{\|} = 8381$ is similar to the value of 8880 (empirical calibration) but smaller than the

value of 9600 (velocity calibration). That the calibrating coefficients depend on different methods demonstrates the fact that precise calibration of a vector magnetograph is very complicated and difficult.

Table 3 Theoretical Calibrating Errors for the Transverse Field

Model	$B1_{\perp}$ (G) 1500	$B2_{\perp}$ (G) 2000
Allen	126	306
DF	13.4	40
VAL-C	19.5	54

In sum, our calibration results should serve as a necessary supplement to the previous calibrations, namely, the empirical calibrations made by Ai (Wang et al. 1996) and the profile and velocity calibrations for the longitudinal field of the photosphere made by Wang, Ai & Deng (1996). In our next work, we will make linear-bias corrections in the data reduction.

Acknowledgements The authors thank the referee for helpful comments and Prof. Deng Yuanyong for discussion. We are indebted to Dr. Liu Jihong for helping improve English writing. We also thank Wang G. P. for her laborious observations. This work was funded by Chinese Academy of Science and the National Natural Science Foundation of China.

References

Ai G., Li W., Zhang H., 1982, Chin. Astron. Astrophys., 6, 39

Allen C. W., 1973, Astrophysical Quantities, The Athlone Press

Balasubramaniam K. S., West E. A., 1991, ApJ, 382, 699

Ding M. D., Fang C., 1989, A&A, 225, 204

Hagyard M. J., Adams M. L., Smith J. E., West E. A., 2000, Solar Phys., 191, 309

Landi Degl'Innocenti E., 1976, A&AS, 25, 235

Landolfi M., Landi Degl'Innocenti E., 1982, Solar Phys., 27, 319

Lites B. W., Skumanich A., 1985, In: M. J. Hagyard, ed., Measurement of Solar Vector Magnetic Fields, NASA CP-2374, p.342

Skumanich A., Rees D. E., Lites B. W., 1985, In: M. J. Hagyard, ed., Measurement of Solar Vector Magnetic Fields, NASA CP-2374, p.306

Vernazza J. E., Avrett E. H., Loeser R., 1981, ApJS, 45, 635

Wallace L., Hinkle K., Livingston W., An Atlas of Sunspot Umbral Spectra in the Visible from 15 000 to 25 500 cm^{-1} (3920 to 6664 Å)

Wang T. J., Ai G. X., Deng Y. Y., 1996, Astrophysics Reports, 23, 31

Wang J. X., Shi Z. X., Wang H. N., Lu Y. P., 1996, ApJ, 456, 861